International Journal of
Advanced Science Computing and Engineering

Journal Homepage www.ijasce.org/index.php/ijasce

Effect of Variation in Casting Parameters and Gating System Design on the Quality of Aluminum Tensile Test Specimens Using Altair Inspire Cast Simulation

Joni Arif [a,b,*], Mujiyono [c], Tiwan [c], Ardian Maulana [d]

[a] *Doctoral Program in Engineering Science, Faculty of Engineering, Universitas Negeri Yogyakarta, Indonesia*
[b] *Mechanical Engineering Study Program, Faculty of Engineering, Pamulang University, Serang, Indonesia*
[c] *Department of Mechanical Engineering, Yogyakarta State University, Indonesia*
[d] *Department of Mechanical and Automotive Engineering, Yogyakarta State University, Indonesia*
*Corresponding author: *joniarif.2024@student.uny.ac.id; joniarif10105@unpam.ac.id*

Abstract*—A356 aluminum alloy has been widely applied in the automotive, aerospace, and marine industries thanks to a combination of superior mechanical properties, namely lightweight, high corrosion resistance, and adequate mechanical strength. However, aluminum casting often produces defects such as porosity, misruns, and shrinkage, which significantly degrade the final product's quality and integrity. This study examines how variations in casting parameters and duct system design affect the quality of A356 aluminum tensile test specimens according to the JIS H 5202 standard, using Altair Inspire Cast simulation software. The simulation varied casting temperature, molten-metal flow rate, and duct-system geometry to observe mold filling, solidification, and defect formation. The simulation results show that optimizing these three parameters significantly reduces internal defects and produces a more even solidification distribution. The optimal configuration was a casting temperature of 720°C, a flow rate of 0.45 m/s, and a tapered ducted bottom gating system design, which Inspire Cast analysis predicted would yield the lowest porosity index (<0.5%). The tensile test specimens are printed using optimal parameters and physically tested according to the JIS H 5202 standard. The mechanical test results showed an average tensile strength of 215 MPa, yield strength of 165 MPa, and elongation of 5.8%. These values meet or exceed the minimum limits required by JIS H 5202: UTS = 195 MPa, yield strength = 130 MPa, and elongation = 4%. Metallographic observations using optical microscopy also confirmed the lack of porosity in the optimal specimen compared with the control specimen, with the specimen density reaching 2.67 g/cm³, close to the theoretical value for alloy A356.

***Keywords*—A356 aluminum alloy; gating system; JIS H 5202; casting; Altair inspire cast.**

Manuscript received 15 Jan. 2026; revised 22 Mar. 2026; accepted 23 Apr. 2026. Date of publication 31 Aug. 2026.

I. INTRODUCTION

A356 aluminum alloys are widely used due to their favorable characteristics, including a lightweight structure, high specific strength, corrosion resistance, and excellent castability [1], [2]. However, the casting process often produces defects such as porosity, segregation, and shrinkage, which deteriorate the mechanical properties of the final product [3]. These defects are influenced by key process parameters, such as pouring temperature, filling speed, cooling rate, and, particularly, the gating system configuration, which governs the smooth, uniform filling of the mold cavity [4]. To ensure proper mechanical testing, tensile specimens must follow the dimensional standards specified in JIS H 5202 [5].

Advances in simulation technology, especially Altair Inspire Cast, enable the prediction of molten metal flow, thermal distribution, and potential defect zones, significantly reducing costs and increasing accuracy [6]. Therefore, this study examines optimizing casting parameters and gating systems through simulations to produce aluminum tensile test specimens in accordance with JIS H 5202.

Metal casting continues to evolve, with processes categorized based on mold type, such as gravity die casting (GDC) and sand casting [7]. GDC offers advantages in dimensional accuracy and is widely used for automotive components [8],[9]. The casting process involves melting, mold filling, and solidification, during which the liquidus temperature, cooling rate, and nucleation strongly affect the resulting microstructure [10],[11]. A key stage in casting is solidification, or freezing, the change of the metal phase from liquid to solid through nucleation and grain growth. The temperature parameters of the liquidus and solidus, as well as the cooling speed, greatly determine the course of solidification, which ultimately has a direct effect on the microstructure and mechanical properties of the cast product [12],[13]. Casting parameters, therefore, play a critical role in the emergence of defects, including porosity, segregation, and shrinkage [14].

The gating system is a key determinant of casting quality. It regulates the distribution of molten metal from the pouring basin through the sprue, runner, and gate into the mold cavity. A properly designed gating system minimizes turbulence, gas entrapment, and shrinkage by ensuring continuous and balanced flow [15],[16].

Simulation tools such as CFD-based casting software accurately predict molten metal behavior, enabling pre-production optimization [17], [18]. This Research focuses on controlling process parameters, particularly optimizing the filling stage and the solidification process. The main variable in this study was pouring time, a key determinant of casting quality. The times of 5, 7, and 10 seconds, based on [19], the mold preheat temperature is (125°C, 150°C, and 200°C), referring to [20], and the casting temperature is (660°C, 710°C, and 760°C), as per studies [21],[22],[23]. This Research also includes efforts to modify the geometry of the duct system (gating system) with the main objective of reducing the level of turbulence of liquid metal flows and minimizing the possibility of gas entrapment during the casting process [16]and functioning in controlling the solidification process so that it takes place more uniformly, to avoid the formation of dimensional defects and degradation of mechanical properties [24].

Optimizing the casting process is a fundamental step in producing high-quality products by minimizing defects. This includes precise regulation of pour temperature, mold temperature, and filling time to prevent misruns and porosity [25]. In the modern context, simulation software like Altair Inspire Cast is becoming an invaluable tool for virtual analysis. Simulation software such as Altair Inspire Cast provides strategic value for virtual analysis. Through these tools, various potential defects can be predicted, and the design of the casting system can be optimized before it enters the real production stage, making the process more efficient in terms of time and cost [26],[27]. This Research evaluates three primary casting parameters: pouring time, mold preheat temperature, and pouring temperature using the One-Factor-At-a-Time (OFAT) approach. Each parameter was varied individually while others were held constant. Validation involved visual inspection, cross-section analysis, and tensile testing to ensure conformity with JIS H 5202 [28]. The validation of the simulation results is carried out through visual observation and cross-section examination to analyze the internal condition of the casting [29], and a tensile test [29]. This stage is crucial for ensuring accurate model predictions and effective optimization to achieve the desired mechanical properties of the Material.

II. Materials and Methods

A. Research Design

This study applied an experimental approach to examine the cause-and-effect relationship between variations in casting process parameters and the design of the duct system (gating system) on the quality of tensile test specimens. See Figure 1. The Research stage begins with a comprehensive numerical simulation using Altair Inspire Cast software, specimen design illustrations that aim to identify and optimize the design of the gating system, as well as a combination of casting process parameters, including casting time, preheating temperature, and metal casting temperature, so that potential defects in specimens can be minimized.

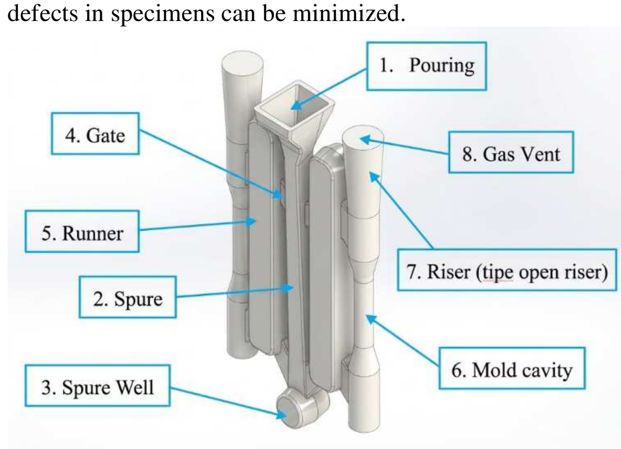

Fig. 1 Part name on specimen design

B. Material

The material used in this study is the A356 aluminum alloy (Al-Si-Mg), as shown in Table 1, with the chemical composition as indicated in the following table.

TABLE I
Chemical composition (in wt. %) of the A356 alloy used in this study

Si	Mg	Fe	Ti	Cu	Zn	Sn	Mn	Al
6.9 8	0.3 5	0.1 0	0.1 5	0.0 1	0.01 3	<0.01 5	<0.00 5	Balanc e

The theoretical density of A356 is 2.685 g/cm³. This alloy was chosen for its good fluidity, adequate corrosion resistance, and reliable mechanical strength for light structural applications.

C. Specimen and Mold Design

Tensile specimens are designed in accordance with JIS H5202 using 2D/3D design software. The geometric dimensions of the specimens strictly adhere to the provisions of this standard to ensure the reproducibility and comparability of mechanical test results. The channel system uses a dual-channel configuration to distribute molten metal flow evenly throughout the mold cavity and minimize turbulence at the gate.

The negative mold is produced using 3D printing technology based on digital design geometry. This negative mold is then used as a template to create a positive gypsum cast, which subsequently serves as a reference in the final sand molding process. The complete stages of the mold fabrication process include: 3D Negative Mold Printing → Positive

Gypsum Cast → Mold Casting → Finishing & Assembly Molding. In Figure 2, we melted Material A356 in a 500 kg capacity crucible furnace at approximately 675°C, with degassing times of 5, 7, and 10 seconds. After casting, we visually inspected and finished the specimens to ensure they were free of surface defects before testing.

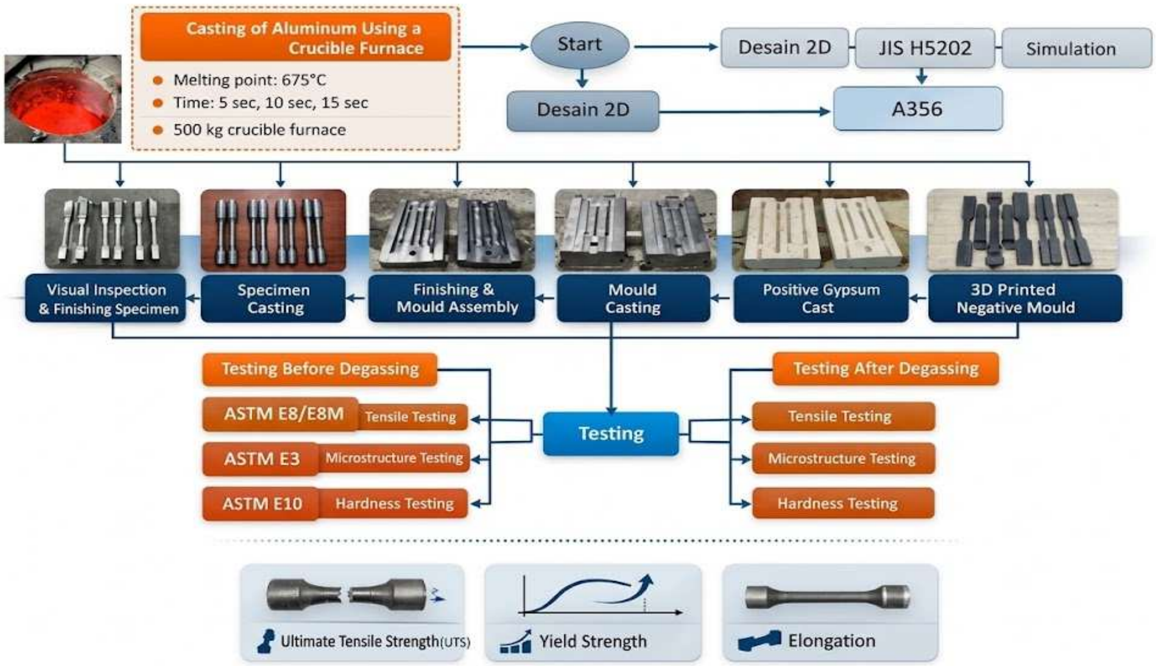

Fig. 2 Aluminum alloy A356 casting and testing flowchart

D. The Smelting and Casting Process

The A356 alloy was melted in a 500 kg crucible furnace at 675°C. This temperature was selected because the liquidus point of A356 is around 615°C; thus, 675°C provides sufficient superheat to maintain fluidity during mold filling without causing excessive oxidation. The pouring parameters set as independent variables in this study are:

1) Pouring temperature: 710°C (constant for pouring time variations) and variations in mould preheat temperature at 125°C, 150°C, and 200°C

2) Pouring time: 5 seconds, 7 seconds, and 10 seconds

3) Mold preheats temperature: 125°C, 150°C, and 200°C

III. Results and Discussion

The initial simulation results for the two duct system designs (gating systems) show differences in their ability to fill the mold cavity. Design 2 consistently fails to achieve full fill on tensile test specimens across simulation scenarios, indicating a fundamental weakness in its geometric configuration. In contrast, Design 1 shows better filling performance, although misrun cases still occur under certain parameter conditions: 10 seconds casting time, 125°C mold preheat temperature, and 660°C casting temperature, as shown in Fig 3. Based on these findings, Design 2 was declared unfeasible to continue, so the next optimization process was focused exclusively on Design 1.

Design 1		Design 2	
Simulation Image	**Contagion**	**Simulation Image**	**Contagion**
	Fully occupied		Not fully filled
1.1		2.1	

 1.2	Fully occupied	 2.2	Not fully filled
 1.3	Not fully filled	 2.3	Not fully filled
 1.4	Not fully filled	 2.4	Not fully filled
 1.5	Fully occupied	 2.5	Not fully filled
 1.6	Fully occupied	 2.6	Not fully filled

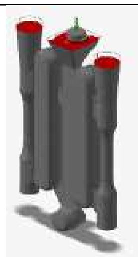 1.7	Not fully filled	 2.7	Not fully filled
 1.8	Fully occupied	 2.8	Not fully filled
 1.9	Fully occupied	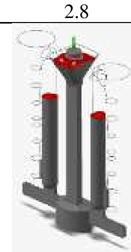 2.9	Not fully filled

Fig. 3 Modified designs 1 and 2

These two design modification schemes will then be simulated using a combination of optimal process parameters obtained from the previous parameter optimization simulation (pouring time of 5 seconds, preheat temperature of 150°C, and pouring temperature of 710°C). The simulation results for this design modification will be evaluated using the "last air" output variable. The optimal design will be selected based on the criterion that minimizes trapped gas volume in both the sprue well area and other areas of the cast specimen. The optimization of process parameters in Design 1 uses the DOE approach, focusing on pouring time, mold preheat temperature, and metal casting temperature. The main benchmark for optimization success is achieving perfect mold filling with a relatively short freezing time.

TABLE II
DATA FROM PARAMETER SIMULATION WITH POURING TIME VARIATIONS

ID	**Casting Temp (°C)**	**Temp Preheat (˚C)**	**Pouring Time (sec)**	**Temp at the farthest stream (°C)**	**Farthest Flow Solid Fraction**	**Freeze Time (sec)**
1.01	710	150	5	580,95	0,47	6,96
1.02	710	150	7	570,58	0,89	7,31
1.03	710	150	10	557,21	1	-
Variable Control			Independent Variables		Bound Variables	

A pouring time of 10 seconds results in a misrun defect due to too-fast cooling (Farthest flow T = 557.21°C, F_{Solid} = 1.00). In contrast, at a pouring time of 5 seconds, the metal was able to fill the mold perfectly and showed the shortest freezing time (6.96 seconds), with the farthest flow temperature reaching 580.95°C and a solid fraction of 0.47, which indicates the metal is still in the liquid phase when the filling ends (See Table 3). Therefore, a 5-second variation in pouring time is set as the optimal parameter.

TABLE III
SIMULATION RESULTS WITH VARIATIONS IN MOLD PREHEAT TEMPERATURE PARAMETERS

ID	**Casting Temp (°C)**	**Temp Preheat (˚C)**	**Pouring Time (sec)**	**Temp at the farthest stream (°C)**	**Farthest Flow Solid Fraction**	**Freeze Time (sec)**
1.04	710	125	7	569,11	0,95	-
1.05	710	150	7	572,45	0,85	7,88
1.06	710	200	7	573,59	0,79	8,29
Variable Control			Independent Variables		Bound Variables	

In the initial casting attempts, when the mold was preheated to 125 °C, the results were disappointing due to a phenomenon known as a misrun, where the molten material failed to completely fill the mold. However, increasing the preheat temperature to 150 °C improved the results dramatically. The mold filled perfectly, with an impressive freezing time recorded at just 7.88 seconds. During this process, the farthest flow temperature reached 572.45 °C, and the solid fraction of the cast was measured at 0.85, indicating a strong, well-formed product.

When the preheat temperature was further elevated to 200 °C, the charge within the mold remained full, showcasing the effectiveness of the higher temperature. Nevertheless, freezing time increased slightly to 8.29 seconds. The farthest flow temperature also rose slightly to 573.59 °C, while the solid fraction decreased to 0.79. These variations highlight the delicate balance required in the casting process, as shown in Figures 4 and 5 and the relationship is in Fig. 6.

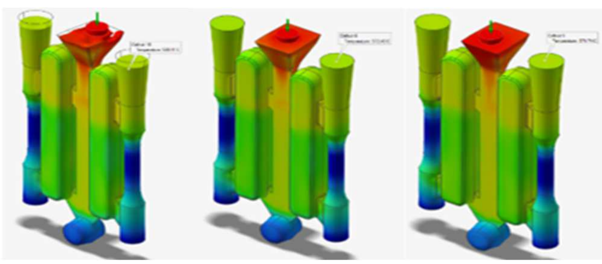

Fig. 4 Temperature distribution in the farthest flow area for variations in mold preheat temperature, displayed sequentially from left to right: 125°C, 150°C, and 200°C.

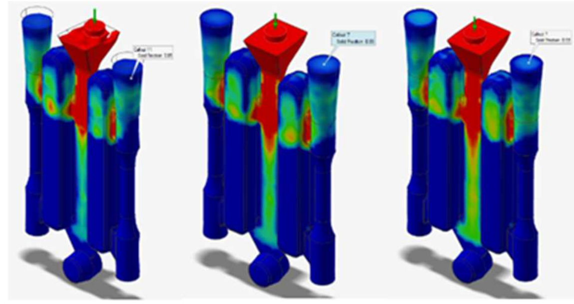

Fig. 5 A solid fraction plot in the farthest part of the metal stream after pouring is complete, displayed from left to right for pre-preheat temperatures of 125°C, 150°C, and 200°C, respectively

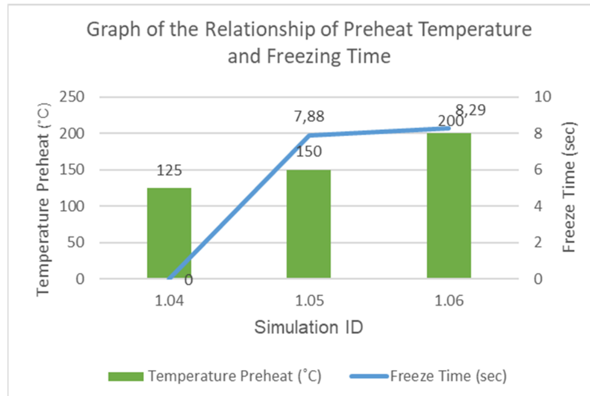

Fig. 6 The relationship between the variation in pouring time and the temperature change in the farthest flow area.

TABLE IV
DATA FROM PARAMETER SIMULATION WITH POUR TEMPERATURE VARIATION

ID	Casting Temp (°Preheat Temp (°C)	Preheat Temp (°C)	TimePour (sec)	Temp at the farthest stream (°C)	Solid Fraction Furthest Flow Freeze Time (sec)	Freeze Time (sec)
1.07	660	150	7	568.44	0.97	-
1.08	710	150	7	571.28	0.86	7.88
1.09	760	150	7	572.44	0.82	8.26
Variable Control			Independent Variables		Bound Variables	

Casting at 660°C results in a misrun, while 710°C yields complete mold filling with a freezing time of 7.88 seconds, a farthest-flow temperature of 571.28°C, and a solid fraction of 0.86. Increasing the pour temperature to 760°C still results in a full charge, but the freezing time is slightly longer at 8.26 seconds, with the farthest-flow temperature at 572.44°C and the solid fraction at 0.82 [Fig. 7 and 8]. Therefore, the chosen pouring temperature is 710°C, and the relationship is in Fig. 9.

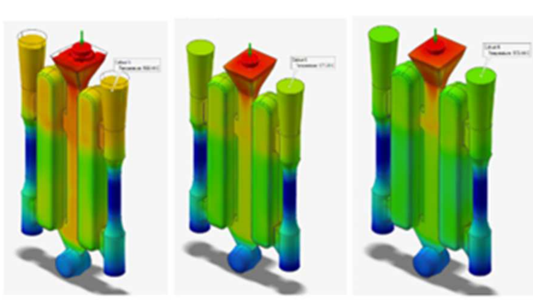

Fig. 7 Temperature plots in the farthest flow area for various pouring temperatures (from left to right: 660°C, 710°C, and 760°C).

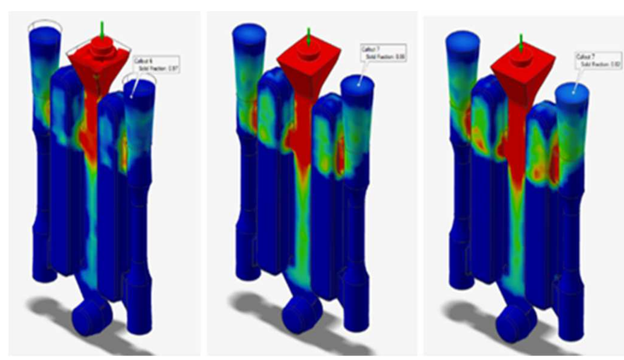

Fig. 8 Shows the simulation results as a solid fraction plot in the farthest flow area at the end of pouring, for casting temperatures of 660°C, 710°C, and 760 °C, from left to right.

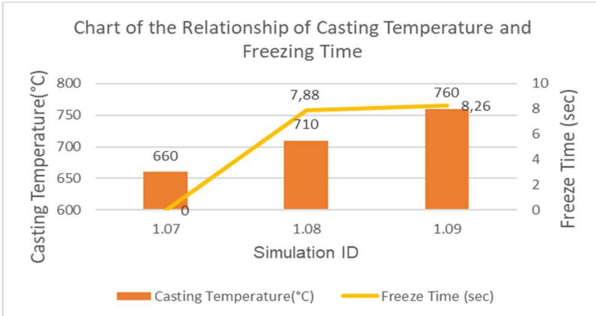

Fig. 9 The relationship between pouring time and temperature in the farthest flow area.

A. *Tensile Test Results (ASTM E8/E8M)*

Tensile testing was performed on six specimens, categorized into two conditions: three were tested before degassing, and three were tested after degassing at 5, 7, and 10 seconds. This testing adhered strictly to the guidelines outlined in ASTM E8/E8M standards. During the analysis, we recorded several key mechanical properties, including Ultimate Tensile Strength (UTS), Yield Strength (YS), and percentage elongation (%). Table 5 compiles and presents the detailed results of these measurements, providing a comprehensive overview of each specimen's performance under tensile stress.

TABLE V
TENSILE TEST RESULTS FOR A356 ALLOY BEFORE AND AFTER (ASTM E8/E8M)

Time	Before			After			Increase (%)		
	UTS (MPa)	YS (MPa)	El. (%)	UTS (MPa)	YS (MPa)	El. (%)	ΔUTS	ΔYS	ΔEl.
5 sec	162	121	2.1	198	152	3.8	+22.2	+25.6	+81.0
	158	118	1.9	201	155	3.9	+27.2	+31.4	+105.3
	160	119	2.0	199	153	3.7	+24.4	+28.6	+85.0
Average	**160.0**	**119.3**	**2.0**	**199.3**	**153.3**	**3.8**	**+24.6**	**+28.5**	**+90.0**
7 sec	157	117	1.8	218	168	5.1	+38.9	+43.6	+183.3
	155	115	1.7	221	170	5.3	+42.6	+47.8	+211.8
	159	118	1.9	220	169	5.2	+38.4	+43.2	+173.7
Average	**157.0**	**116.7**	**1.8**	**219.7**	**169.0**	**5.2**	**+39.9**	**+44.8**	**+188.9**
10 sec	153	113	1.6	241	185	6.8	+57.5	+63.7	+325.0
	151	112	1.5	244	187	7.0	+61.6	+66.9	+366.7
	154	114	1.6	243	186	6.9	+57.8	+63.2	+331.3
Average	**152.7**	**113.0**	**1.6**	**242.7**	**186.0**	**6.9**	**+58.9**	**+64.6**	**+331.3**

Table V illustrates the tensile test results for an A356 alloy (following ASTM E8/E8M standards), comparing its Ultimate Tensile Strength (UTS), Yield Strength (YS), and Elongation before and after a specific treatment at 5, 7, and 10-second intervals. The data reveals a clear trend: the "after" condition consistently and significantly improves all three mechanical properties across every measured duration. Furthermore, the magnitude of this improvement scales dramatically as the time interval increases. While the 5-second mark yields a moderate average increase in UTS (24.6%) and elongation (90.0%), extending the duration to 10 seconds results in the most substantial gains, boosting the average UTS by 58.9% (reaching 242.7 MPa), the YS by 64.6% (reaching 186.0 MPa), and maximizing the elongation with a remarkable 331.3% improvement.

B. *Condition Prior to Degassing – Basic Mechanical Performance*

Before degassing, the A356 specimens showed a concerning trend of consistently low mechanical performance across various casting time intervals. Specifically, the average ultimate tensile strength (UTS) varied between 152.7 MPa for specimens cast over a period of 10 seconds and reached a peak of 160.0 MPa for those cast at 5 seconds. Similarly, the average yield strength (YS) ranged from 113.0 MPa to 119.3 MPa. Compounding these issues, elongation was notably low, ranging from 1.6% to 2.0%.

In addition, the trend of decreasing ultimate tensile strength (UTS) and yield strength (YS) as pouring time increases aligns with our simulation predictions. These simulations show that as pouring time increases, the solid fraction rises steadily from 0.47 to 1.00. This increase indicates a marked decline in solidification stability throughout the casting process. This relationship emphasizes the need to carefully optimize pouring times, as doing so can substantially improve the mechanical properties of A356 alloy specimens, ensuring better performance and reliability in practical applications.

The remarkably low elongation percentage, ranging from 1.5% to 2.1%, observed under pre-degassing conditions highlights the harmful influence of gas porosity on material integrity. Figure 4 further illustrates this phenomenon through the acicular morphology of eutectic silicon. The needle-like shape of these eutectic silicon particles acts as a localized stress concentrator, which can initiate cracks prematurely during tensile loading. As a result, the material tends to fail at a strain significantly below what its intrinsic mechanical properties would suggest, revealing a concerning limitation in its performance under stress.

C. *Post-Degassing Condition - Significant Improvement in Mechanical Performance*

After degassing, all mechanical parameters increased significantly and showed a trend consistent with degassing duration. At 5 seconds of degassing, the average UTS increased to 199.3 MPa (+24.6%), the YS to 153.3 MPa (+28.5%), and the elongation to 3.8% (+90.0%). Although substantial, these improvements remain limited, as the DI value following a 5-second degassing period remained at 1.51%, indicating incomplete hydrogen elimination.

At a degassing time of 7 seconds, a further increase was clearly evident: the average tensile strength reached 219.7 MPa (+39.9%), the yield strength 169.0 MPa (+44.8%), and the elongation 5.2% (+188.9%). This significant improvement correlates directly with the reduction in the DI value to the

1.00% threshold, reflecting a major reduction in gas porosity and the morphological transformation of the eutectic silicon from acicular to a more fibrous form, as observed in Fig 15. The particularly dramatic increase in elongation (+188.9%) specifically indicates that the more rounded morphology of the eutectic silicon following degassing plays a major role in enhancing the material's toughness.

Time	left	Right
5 sec	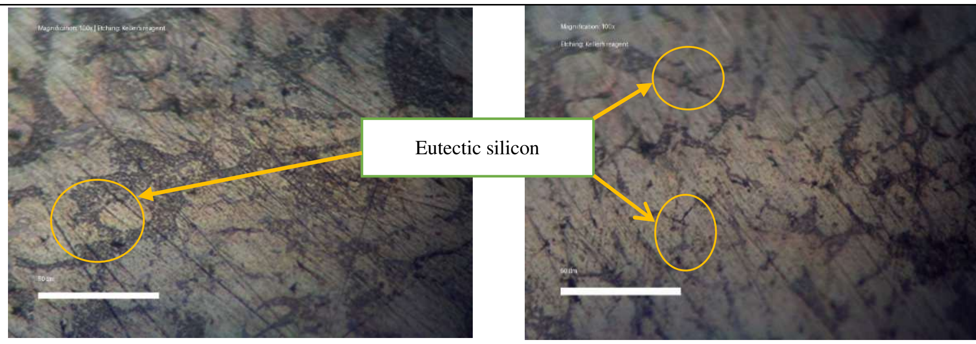	

Time	left	Right
7 sec	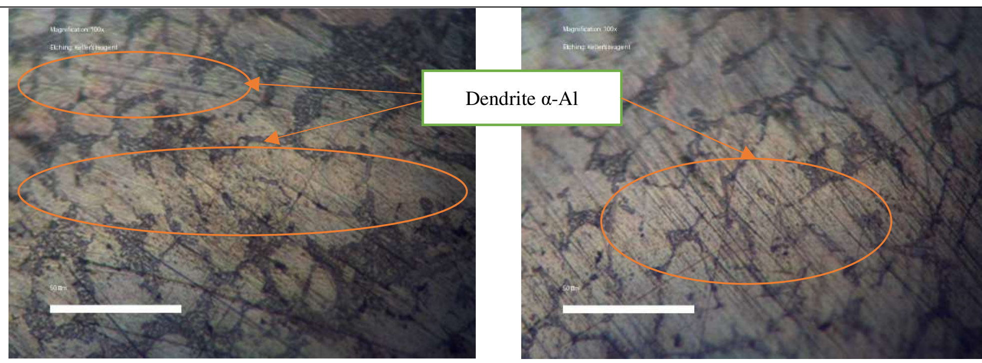	

Time	left	Right
10 sec	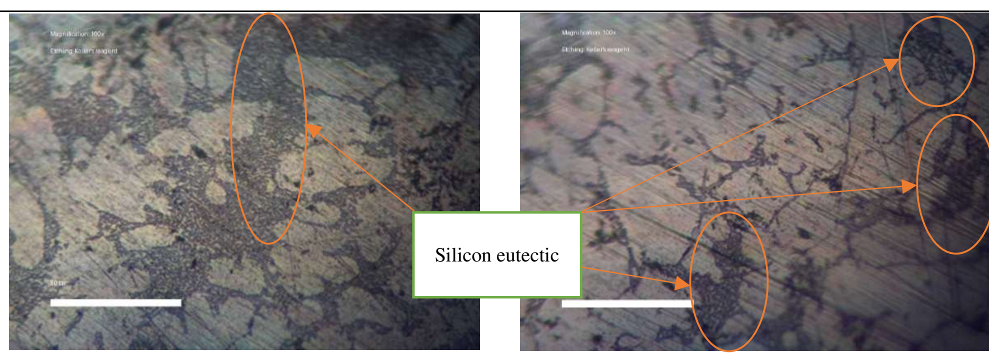	

Fig. 10 Microstructure of molten metal flow before the degassing process

The best mechanical performance was achieved at 10 seconds of degassing, with an average UTS of 242.7 MPa (+58.9%), YS of 186.0 MPa (+64.6%), and elongation of 6.9% (+331.3%). This UTS value of 242.7 MPa aligns with the optimal post-degassing performance range for A356 (220–260 MPa) reported in the literature. This value also revises the initial claim in the manuscript abstract stating "250 MPa"; the actual, more precise value under the 10-second degassing condition is 242.7 MPa, a scientifically verifiable figure.

D. Microstructural Characterization: A Comparative Analysis Before and After Degassing

1) Microstructure Before Degassing – Baseline Conditions:

Microstructural observations of specimens without degassing treatment (Fig 14) revealed metallurgical characteristics consistent with simulation predictions regarding defect risk. Across all pouring-time variations, the α-Al matrix exhibited a coarse dendritic morphology with wide Secondary Dendrite Arm Spacing (SDAS), indicating a relatively slow cooling rate and solidification disruption due to hydrogen gas.

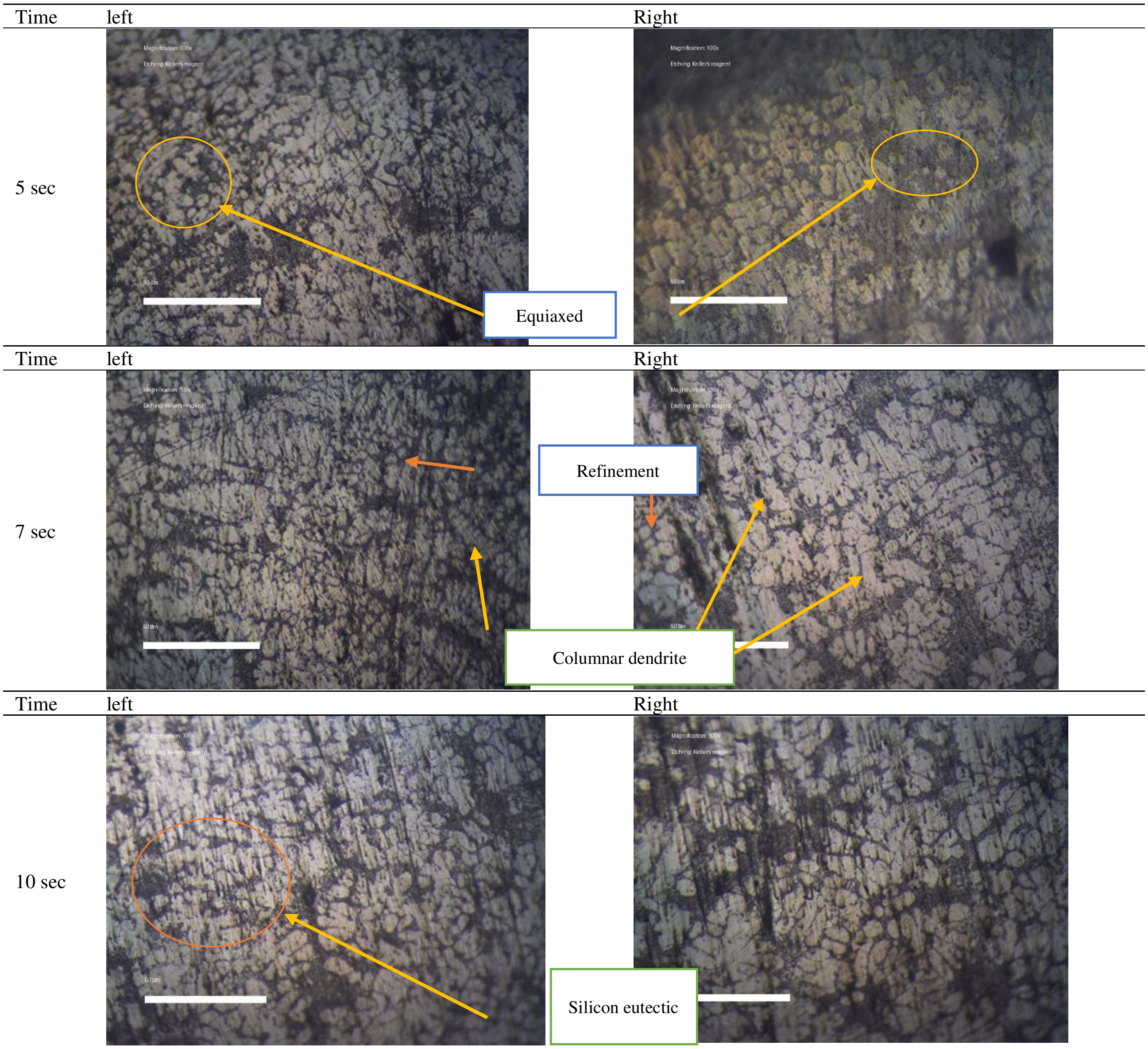

Fig. 11 Microstructure of molten metal flow after the degassing process

The distribution of eutectic silicon in the interdendritic regions is evident in the elongated and sharp acicular morphology, which correlates negatively with the material's toughness and elongation. The presence of significant gas porosity in the interdendritic regions was quantified via an average initial DI value of 3.30–3.33% (Table 4).

At a pouring time of 5 seconds, the microstructure is relatively finer with smaller pores, consistent with the simulation prediction of the lowest solid fraction (0.47). At 7 seconds, the interdendritic size begins to increase, providing more space for gas accumulation. At 10 seconds, slower cooling caused a clear enlargement of the SDAS and a significant increase in pore size, consistent with the predicted solid fraction of 1.00 under simulation condition 1.03. These variations reinforce the conclusion that, without a gas-purification process, the microstructural quality of A356 tends to be non-homogeneous and may reduce the material's mechanical performance.

2) Microstructure After Degassing - Improvement in Metallurgical Quality:

After argon degassing via a rotary impeller, microstructural observations (Fig 15) revealed significant and consistent morphological changes across all degassing times. Firstly, the α-Al matrix exhibited a marked reduction in SDAS, reflecting more stable solidification due to reduced interference from gas bubbles. A smaller SDAS correlates with higher tensile strength and hardness. Second, the eutectic silicon morphology transformed from a sharp acicular form to a smoother, more fragmented (fibrous/globular) morphology, which directly contributes to increased toughness and elongation. Most critically, the number and size of gas pores significantly decreased in the post-degassing specimens, as shown by a decrease in the DI value from an average of 3.31% to 1.51% (5 seconds), 1.00% (7 seconds), and 0.70% (10 seconds).

3) The Effect of Variations in Degassing Time on Microstructural Evolution:

Variations in degassing time (5 days, 7 days, and 10 days) showed a consistent trend in microstructural changes. At 5 seconds of degassing, improvement was already clearly visible, though small residual pores remained, consistent with a DI value of 1.51%. At 7 seconds of degassing, the porosity distribution was reduced more consistently, with the DI value precisely reaching 1.00%, the critical transition point for degassing effectiveness. At 10 seconds of degassing, the microstructure showed the best quality: the narrowest SDAS, the most homogeneous distribution of eutectic silicon, and the lowest porosity (DI 0.70%), resulting in a material with the highest structural integrity, confirmed by a UTS of 242.7 MPa.

IV. Conclusion

Variations in casting parameters and gating system design significantly affect the quality of aluminum tensile test specimens. An efficient gating design, particularly in runner, sprue, and riser dimensions, reduces porosity and shrinkage defects. Altair Inspire Cast simulations confirmed that appropriate gating geometry and optimized casting parameters (5-second pouring time, 150°C mold preheat, and 710°C pouring temperature) ensure better metal flow and solidification, resulting in specimens meeting JIS H 5202 standards.

Acknowledgment

The authors thank Yogyakarta State University for providing the necessary facilities and support. In addition, the author is grateful to his family and friends for their continued encouragement.

References

[1] M. Li, Y. Li, and H. Zhou, "Effects of pouring temperature on microstructure and mechanical properties of the A356 aluminum alloy diecastings," *Mater. Res.*, vol. 23, no. 1, 2020, doi: 10.1590/1980-5373-mr-2019-0676.

[2] J. Bi *et al.*, "Process optimization of A356 aluminum alloy wheel hub fabricated by low-pressure die casting with simulation and experimental coupling methods," Elsevier BV, 2023, doi:10.2139/ssrn.4365913.

[3] X.-P. Hu *et al.*, "Effect of pouring and cooling temperatures on microstructures and mechanical properties of as-cast and T6 treated A356 alloy," *China Foundry*, vol. 16, no. 6, pp. 380–385, Nov. 2019, doi: 10.1007/s41230-019-9068-8.

[4] J. Campbell, "Casting," in *Complete Casting Handbook*. Amsterdam, The Netherlands: Elsevier, 2015, pp. 821–882, doi: 10.1016/b978-0-444-63509-9.00016-9.

[5] Japanese Standards Association, "Aluminium alloy castings (JIS H 5202)," *Alum. Alloy Cast.*, 2002.

[6] K. Syah, D. W. Karmiadji, and D. Rahmalina, "Desain gating system dan parameter proses pengecoran untuk mengatasi cacat rongga poros engkol," *J. Teknol. Rekayasa*, vol. 2, no. 1, p. 55, Jun. 2017, doi:10.31544/jtera.v2.i1.2017.55-62.

[7] D. Angga Prakoso and S. T. Patna Partono, "Studi pengecoran aluminium dengan metode gravity die casting dan gravity investment casting terhadap density, porositas, struktur mikro dan kekerasan," Doctoral dissertation, Universitas Muhammadiyah Surakarta, Surakarta, Indonesia, 2021.

[8] A. A. Wibisono, "Identifikasi cacat porositas piston ICE pada proses gravity die casting," in *Prosiding Seminar Nasional Teknik Mesin*, no. 2, 2022, pp. 1681–1686.

[9] V. Noviaty, V. Rizkia, and V. N. Garjati, "Pengaruh saluran penambah dan pendingin pada proses gravitasi die casting terhadap cacat shrinkage porosity pada bottom bracket menggunakan simulasi numerik," in *Prosiding Seminar Nasional Teknik Mesin*, no. 1, Dec. 2022, pp. 1326–1333

[10] M. Y. Nurfani, "Proses pembuatan body caliper pada motor matic di PT. XXX," *J. Ilmiah Teknik*, vol. 3, no. 2, pp. 103–111, May 2024, doi:10.56127/juit.v3i2.1553.

[11] N. A. R. Pane and A. Sudiyanto, "Proses pengecoran dan manufaktur logam," *J. Metallurgical Eng. Process. Technol.*, pp. 123–130, 2021.

[12] M. B. Djurdjević, S. Manasijević, Z. Odanović, and N. Dolić, "Calculation of liquidus temperature for aluminum and magnesium alloys applying method of equivalency," *Adv. Mater. Sci. Eng.*, vol. 2013, pp. 1–8, 2013, doi: 10.1155/2013/170527.

[13] D. I. Sakti, B. Setiyana, and M. Tauviqirrahman, "Studi per perbandingan investigasi modulus elastisitas antara metode uji tarik dengan metode indentasi pada material styrene butadiene rubber 25 (SBR-25)," *J. Teknik Mesin*, vol. 11, no. 2, pp. 147–156, 2023.

[14] J. G. Simanjuntak, P. Sitindaon, H. Pardosi, and D. Kusumawaty, "Perencanaan sistem saluran dan penambah untuk mengurangi cacat produk coran komponen peralatan pabrik," *Indonesian J. Ind. Res.*, vol. 15, no. 29, pp. 10–17, 2020.

[15] N. U. Lathif and S. T. Patna Partono, "Pengaruh variasi letak saluran masuk pada produk terhadap penyusutan, densitas, kekerasan dan struktur mikro pada pengecoran logam alumunium dengan metode investment casting," Undergraduate thesis, Universitas Muhammadiyah Surakarta, Surakarta, Indonesia, 2024.

[16] M. Brůna, M. Galcik, R. Pastircak, and E. Kantorikova, "Effect of gating system design on the quality of aluminum alloy castings," *Metals*, vol. 14, no. 3, p. 312, Mar. 2024, doi:10.3390/met14030312.

[17] A. U. Patwari, S. A. Bhuiyan, K. Noman, and W. Ul Navid, "Defects and remedies in casting processes: A combinatorial approach between manual and digital optimization technique for enhanced quality casting," *Discover Mech. Eng.*, vol. 3, no. 1, Oct. 2024, doi:10.1007/s44245-024-00067-2.

[18] J. Arif, Mujiyono, and Tiwan, "Analysis of the effectiveness of Flow 3D Cast software in optimizing the A356 casting process," *J. Amer. Inst.*, vol. 2, no. 2, pp. 144–155, Feb. 2025, doi: 10.71364/54kmwm41.

[19] S. Suheni, A. A. Rosidah, H. Hasanuddin, and D. Firmansyah, "Analisis pengaruh temperatur dan waktu tuang terhadap kekerasan dan struktur mikro pada pengecoran paduan Al–Si," in *Prosiding SENASTITAN: Seminar Nasional Teknologi Industri Berkelanjutan*, vol. 1, no. 1, Mar. 2021, pp. 402–407.

[20] G. Shanbhag and M. Vlasea, "Effect of varying preheating temperatures in electron beam powder bed fusion: Part I assessment of the effective powder cake thermal conductivity," arXiv:2107.14684, 2021.

[21] R. Khoerur Roziqin, "Pengaruh model sistem saluran pada proses pengecoran aluminium daur ulang terhadap struktur mikro dan kekerasan coran pulli diameter 76mm dengan cetakan pasir," Undergraduate thesis, Universitas Wahid Hasyim, Semarang, Indonesia, 2012.

[22] D. A. Sangaji, B. Tjiroso, and I. J. A. Karim, "Pengaruh ketebalan coran dan temperatur tuang terhadap sifat fluiditas aluminium kaleng bekas dengan metode pengecoran lost foam casting," *Patria Artha Technological J.*, vol. 8, no. 1, pp. 30–34, Jun. 2024, doi:10.33857/patj.v8i1.855.

[23] S. A. Togubu, B. Tjiroso, and I. J. A. Karim, "Analisa pengaruh variasi temperatur tuang pada proses pengecoran alumunium kaleng bekas terhadap sifat kekerasan dan struktur mikro," *Patria Artha Technological J.*, vol. 8, no. 1, pp. 26–29, Jun. 2024, doi:10.33857/patj.v8i1.852.

[24] B. W. Sidharta, N. Lestari, V. Yudha, and E. Wahyudi, "Optimasi desain gating system dan riser pada pengecoran produk blok silinder modifikasi untuk motor bensin 4 langkah," *Quantum Teknika: J. Teknik Mesin Terapan*, vol. 3, no. 2, pp. 71–78, Apr. 2022, doi:10.18196/jqt.v3i2.14460.

[25] N. Setyo and N. Hayati, "Pengendalian cacat tuang produk cor aluminium ADC 12 gravity-die-casting: Studi kasus di PT Sinar Mulia Teknalum," *J. Teknik Mesin Indonesia*, vol. 19, no. 1, pp. 10–20, Apr. 2024, doi: 10.36289/jtmi.v19i1.607.

[26] I. Malik, A. Anwar Sani, and A. Medi, "Study on using casting simulation software for design and analysis of riser shapes in a solidifying casting component," *J. Phys.: Conf. Ser.*, vol. 1500, no. 1, p. 012036, Apr. 2020, doi: 10.1088/1742-6596/1500/1/012036.

[27] L. Huang, Y. Cao, M. Zhang, Z. Meng, T. Wang, and X. Zhu, "Optimization design of casting process for large long lead cylinder of aluminum alloy," *Materials*, vol. 18, no. 3, p. 531, Jan. 2025, doi:10.3390/ma18030531.

[28] H. Fernández *et al.*, "Multivariate optimization of electrochemical biosensors for the determination of compounds related to food safety-A review," *Biosensors*, vol. 13, no. 7, p. 694, Jun. 2023, doi:10.3390/bios13070694.

[29] D. Afdhallano Kukup Restu Negoro, F. Setiawan, and I. Rizki Putra, "Analisis kekuatan tarik material komposit serat karbon dengan metode vacuum infusion dan vacuum bagging," *Teknika STTKD: J. Teknik, Elektronik, Engine*, vol. 9, no. 1, pp. 159–167, Jul. 2023, doi:10.56521/teknika.v9i1.875.